THE JOURNAL OF PHYSICAL CHEMISTRY Letters

Letter

pubs.acs.org/JPCL

# Charge Transport Limitations in Self-Assembled $TiO_2$ Photoanodes for Dye-Sensitized Solar Cells

Pablo Docampo,[†] Stefan Guldin,[‡] Ullrich Steiner,[‡] and Henry J. Snaith*,[†]

[†]Clarendon Laboratory, University of Oxford, Parks Road, OX1 3PU, Oxford, United Kingdom

[‡]Department of Physics, University of Cambridge, J. J. Thomson Avenue, Cambridge, CB3 0HE, United Kingdom

Supporting Information

**ABSTRACT:** Solid-state dye-sensitized solar cells offer the possibility of high-power conversion efficiencies due to theoretically lower fundamental losses in dye regeneration. Despite continuous progress, limitations in charge diffusion through the mesoporous photoanode still constrain the device thickness and hence result in reduced light absorption with the most common sensitizers. Here we examine block copolymer-assembled photoanodes with similar surface area and morphology but a large variation in crystal size. We observe that the crystal size has a profound effect on the electron transport, which is not explicable by considering solely the ratio between free and trapped electrons. Our results are consistent with the long-range mobility of conduction band electrons being strongly influenced by grain boundaries. Therefore, maximizing the crystal size while maintaining high enough surface area will be an important route forward.

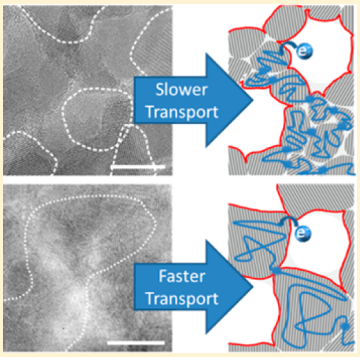


**SECTION:** Energy Conversion and Storage; Energy and Charge Transport

The dye-sensitized solar cell (DSC) has attracted widespread interest by research and industry alike since its introduction by O'Regan and Grätzel in 1991.[1,2] Replacing the standard redox systems of $I^-/I^{3-}$ liquid electrolyte by an organic solid-state molecular hole-conductor[3] may, in principle, allow significantly higher open circuit voltage with maximum theoretical power conversion efficiency of over 20%.[4] In practice, solid-state devices have been reported to surmount 7% efficiencies.[5] To experimentally approach predicted efficiency values, we must identify the limiting factors for device performance. In related studies, the comparatively low photocurrent of the solid-state DSCs was attributed to poor wetting and pore filling of the mesoporous network by the solid-state hole conductor, typically (2,2(7,7(-tetrakis-(*N*,*N*-dipmethoxyphenylamine)9,9(-spirobifluorene) Spiro-MeO-TAD).[6−9] However, recent studies have found that sufficient (>60%) pore-filling with the current state-of-the-art materials is feasible for electrode thicknesses up to 5 $\mu$m and hence, we consider other limiting factors.[10,11]

Both solid-state and liquid electrolyte DSCs suffer from slow electron diffusion through the porous titania under short-circuit conditions due to its low charge density.[12−14] Provided the conductivity of the hole-transporter is over $10^{-6}$ S $cm^{-1}$, the particular choice of hole transporter is not expected to have significant impact on transport at short circuit.[15] Alternative photoanode materials for DSCs with higher electron mobilities and suitable energy levels of conduction and valence band are ZnO[16−18] and $SnO_2$.[19,20] The bulk mobility for these two materials is ∼200 $cm^2V^{-1}s^{-1}$,[21,22] nearly two orders of magnitude higher than for $TiO_2$.[23] Nevertheless, the electron transport dynamics are very similar in nanoparticle assemblies of these oxides.[24−27] In fact, changes to the diffusion coefficients seem to correlate to the crystal size of the mesoporous oxide[26,28−32] rather than to its morphological arrangement or material type,[33,34] as long as the porosity is sufficiently low (<50−60%).[35,36] Here we undertake a systematic investigation of the transport limitations in mesoporous photoanodes by studying a series of block copolymer-structured $TiO_2$ photoanodes. This fundamentally different approach allows us to compare photoanodes of similar morphology and surface area, but a largely different mean crystal size. We observe for the first time a strong dependence of electron diffusion with grain boundary density, highlighting the importance of long-range crystallinity in mesoporous photoanodes.

The electron transport in mesoporous, nanocrystalline photoanodes is generally described by a multiple-trapping model.[37,38] Upon generation of an excited state in the dye, electrons are transferred into the mesoporous oxide where they relax and become localized in sub-bandgap states. Electron transport then occurs in an iterative fashion of thermal detrapping, diffusion in the conduction band and retrapping. In this way, transport is moderated by detrapping times, which are longer for deeper traps.[39−42] The conductivity of the films, and hence charge transport, directly depends on the occupancy of electrons in the conduction band $n_{FREE}$, which in turn is determined by the trapped charge density $n_{TRAP}$, the effective

**Received:** January 14, 2013
**Accepted:** January 30, 2013

   dx.doi.org/10.1021/jz400084n | *J. Phys. Chem. Lett.* 2013, 4, 698−703

density of conduction band states $N_{CB}$, and the total trap density $N_{tot}$ in the film as[42]

$$n_{FREE}^{\alpha} = \frac{N_{CB}^{\alpha}}{N_{tot}} n_{TRAP} \quad (1)$$

where $\alpha$ is related to the shape and distribution of sub bandgap states.

Clearly, if the trap density is reduced, then an increase in the free electron density at the same quasi Fermi level should follow, and hence a faster "average" transport should be achieved. It is therefore important to understand the nature and location of the trap states.

Kopidakis et al. have performed a study to infer the spatial location of transport-limiting traps in a colloidal nanoparticle-based mesoporous photoanode and resolve whether they are mainly located at the particle's surface, in the bulk, or at the grain boundaries.[29] By characterizing photoanodes composed of different $TiO_2$ particle sizes and therefore surface areas and estimating the required number of traps to account for the observed transport characteristics, they found a consistent correlation if the transport limiting traps were mainly located on the exposed surface. An argument was also put forward that if the transport-limiting traps were located at the intergrain boundaries, then the total trap density should depend linearly on the number of particles in the film. This hypothesis, however, does not take into account the variability of the interparticle contact area. We believe that the internal surface area between the grains may represent another important parameter, possibly indistinguishable from the effect of traps located on the exposed surface area.

It is very challenging to disentangle the change in exposed surface area from changes in interparticle contact area when using conventional colloidal nanocrystals, as the exposed surface area of the porous films is inherently related to the crystal size. The structure formation process of block copolymer-directed inorganic films is fundamentally different and has recently led to promising results when used as photoanodes in solid-state DSCs.[43,44] The pore size and film can be controlled by the block copolymer structure and the oxide sol to copolymer ratio,[45,46] whereas the crystal size can be independently governed by temperature-induced crystallization.[43,47] We have therefore employed this copolymer approach to study the charge transport in nanocrystalline $TiO_2$ (see the Experimental Section). Figure 1a,c shows high-resolution TEM images of the formed structure for substrates calcined at 400 and 650 °C, and Figure 1b,d depicts a schematic 2D cross-section of the corresponding films. The change of crystal size and shape is clearly discernible from the TEM images. Further characterization was previously performed by X-ray diffraction (XRD), shown in Figure 1e, and dye desorption, shown in Figure 1f, to quantify crystal size and accessible surface area of the samples, respectively.[43] It was found that the only crystal phase present in all of the prepared samples up to 700 °C was anatase.[43] Samples calcined at temperatures between 400 and 500 °C exhibited randomly distributed crystals that are significantly smaller than the wall thickness of the porous template. For samples calcined at 650 °C and beyond, the crystal size exceeded the wall thickness of the template-dictated confinement, resulting in anisotropic growth within the network as well as showing a significant reduction in available surface area for dye anchoring. All samples prepared in this study exhibited a similar film porosity of under 40%, as previously determined.[43] To keep the exposed surface area invariant between samples, only films calcined below 650 °C have been considered here.

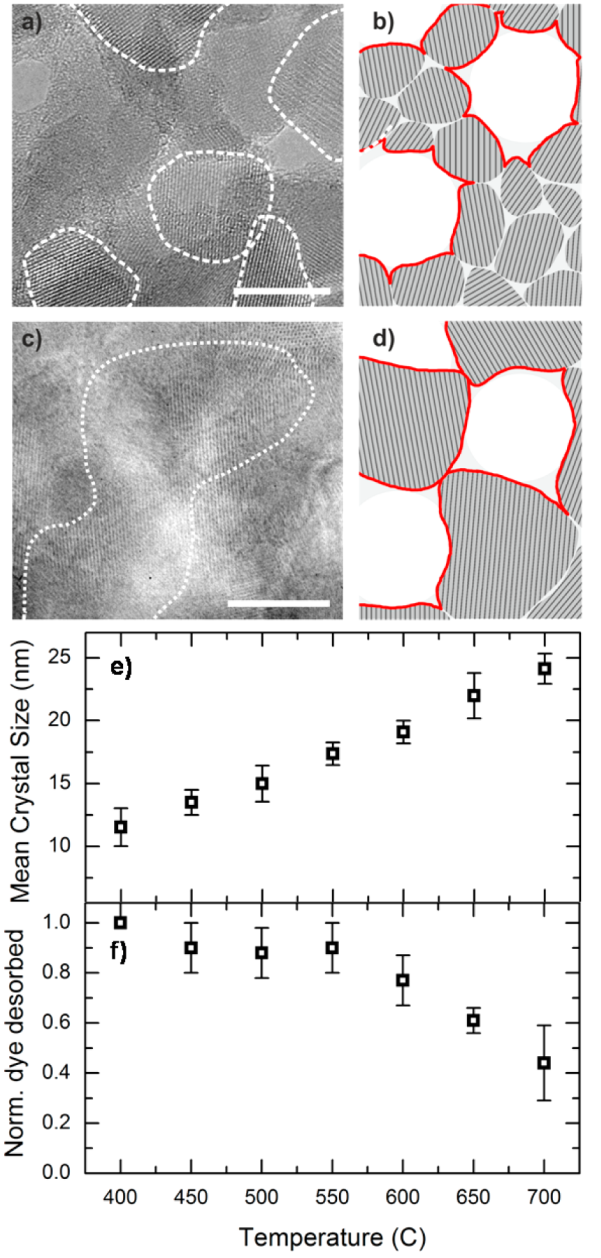


**Figure 1.** Assembly of nanocrystals within the mesoporous $TiO_2$ network. Left: High-resolution transmission electron microscopy images (HRTEM) of samples crystallized at 450 (a) and 650 °C (c). Scale bars represent 10 nm. For guidance, white dotted lines are superimposed to visualize the individual crystallites. Right: Schematic of the observed crystallite assembly at 450 (b) and 650 °C (d). (e) Crystallite size and (f) normalized surface area as a function of calcination temperature. The data in this Figure are adapted with permission from ref 43.

Changes to the surface properties of the photoanodes are usually reflected in the density of sub-bandgap states of the material.[32,48] Although the variation in calcination temperatures here results in largely different crystal sizes, the available surface area for dye-anchoring has been kept relatively invariant. We do not therefore expect a significant shift in the sub-bandgap density of states (DoS) as observed for colloidal approaches.


dx.doi.org/10.1021/jz400084n | J. Phys. Chem. Lett. 2013, 4, 698−703

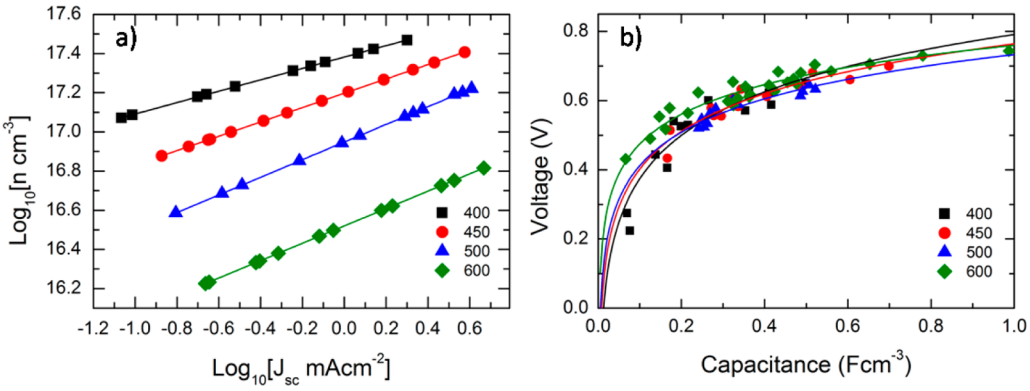


**Figure 2.** Log–log plot of charge density ($n$) against short circuit current ($J_{SC}$) (a) and voltage against capacitance (b) for photoanodes that were exposed to a range of calcination temperatures.

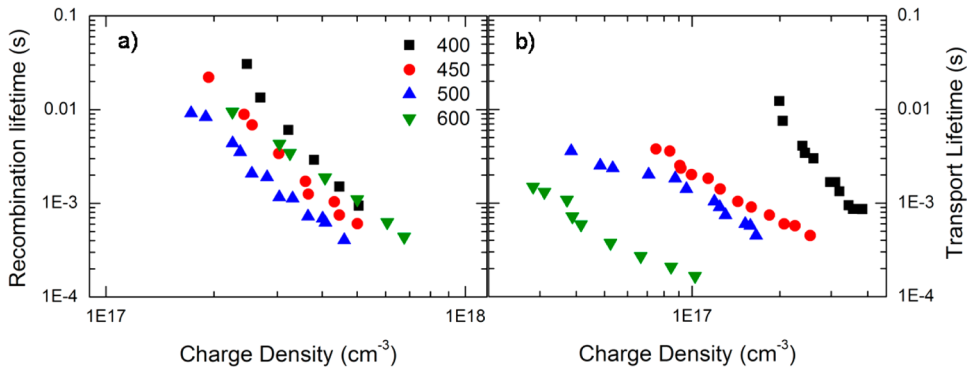


**Figure 3.** (a) Photovoltage decay and (b) photocurrent decay plotted against charge density for photoanodes that were subjected to a range of calcination temperatures.

To study the electronic properties of the photoanodes, solar cells were constructed by sensitizing the films with the organic dye D102 and infiltrating them with the hole-conductor spiro-OMeTAD. They were then characterized through transient photovoltage and photocurrent decay measurements. (See the Supporting Information.)

The DoS of the fabricated solar cells is expected to vary exponentially, and hence the relative changes between the total trap density of the different samples can be quantified by extracting the charge density under short-circuit conditions and comparing this value with the short-circuit current flowing through the device.[49,50] Such a plot is presented in Figure 2a. The data suggest an almost one order of magnitude difference in the total trap density between samples calcined at 400 and at 600 °C. Hypothetically, this could lead us to postulate that the "transport limiting traps" are located at the grain boundaries rather than at the nanoparticle surface. However, this does not seem to be the case. Changes in the total trap density should also be reflected in a capacitance versus voltage plot, as shown in Figure 2b, where we observe that the capacitances of all samples overlap, indicating an absence of a major change in the trap density. This apparent inconsistency suggests that the trend observed in Figure 2a arises from another previously unconsidered phenomenon. To further investigate, charge transport and recombination measurements were also performed via the photovoltage and photocurrent decay technique.

From the photovoltage decay measurements and integrating the DoS presented in Figure 2b, the recombination lifetime and its dependence on charge density can be extracted (see the Supporting Information). These results are shown in Figure 3a. No significant trend is observed, with all data sets showing a similar dependence on charge density. This is consistent with our assumption of a comparable surface area for all the films because recombination must occur at or across the dye-sensitized heterojunction and is hence proportional to its interfacial area.[51] Interestingly, however, the transport characteristics between the different samples are vastly different: Figure 3b exhibits a highly significant enhancement of electron transport with increasing crystallization temperature and hence with crystal size. In fact, the transport lifetime at constant charge density of $\sim 10^{17}$ cm$^{-3}$ varied by more than two orders of magnitude. The fact that transport varied greatly while recombination dynamics stayed relatively unchanged in the present series of experiments is in contradiction to the assumption of "transport-limited" recombination. This was proposed in several publications, where faster transport was postulated to result in higher recombination as charges encounter recombination sites more frequently.[14,52]

The results presented in Figure 3 can now explain the trend observed in Figure 2a, since the charge density in the film under short circuit conditions $n_{SC}$ is proportional to the short circuit current $J_{SC}$ and the charge collection lifetime $\tau_c$:[14,53]

$$n_{SC} \propto J_{SC}\tau_c \quad (2)$$

The fact that electron transport varied so greatly with calcination temperature while the DoS remained relatively invariant is very surprising. From the multitrapping model, it is assumed that the transit time between traps is negligible compared with the trapping time. Hence, only materials with very different trapping densities are expected to exhibit


dx.doi.org/10.1021/jz400084n | J. Phys. Chem. Lett. 2013, 4, 698–703

significantly dissimilar charge-transport characteristics. Because the total trap density does not seem to vary significantly for the photoanodes presented here we must look elsewhere to understand the changes in transport and the charge density dependence of the short-circuit current.

From multitrapping models, the charge collection lifetime $\tau_c$ can be written as[14,53]

$$\tau_c \approx 2.55 C d^2 N_{CB}^{-kT/m_c} N_{tot}^{2/3} (kT v_c \sigma_c)^{-1} \left( \frac{I_0 f_\alpha}{\alpha_b D_{n,free}} \right)^{kT/m_c - 1} \quad (3)$$

where $C$ is a proportionality constant, $d$ is the thickness of the film, $m_c$ is the average trap depth, $v_c$ is the free electron velocity, $\sigma_c$ is the trap capture cross section, $I_0$ is the light intensity, $\alpha_b$ is the dye absorption coefficient, $f_\alpha$ is a factor that depends only on how light is absorbed, $k$ is Boltzmann's constant, $T$ is the temperature, and $D_{n,free}$ is the free electron diffusion coefficient.

For the material system presented here, neither the total trap density nor the surface area available for dye adsorption varies significantly with sintering temperature. In contrast, the crystal sizes shows a strong dependence on calcination temperature, and it is reasonable to assume that the free electron velocity $v_c$ and diffusion coefficient $D_{n,free}$ are variable with crystal size,[54] both of which are proportional to the free electron mobility $\mu_e$. Following on from eq 3, the charge collection time $\tau_c$ decreases with increasing free electron mobility as

$$\tau_c \propto \mu_e^{-kT/m_c} \quad (4)$$

It has previously been shown for polycrystalline semiconductors that the crystal grain size can have a strong influence on the long-range mobility of electrons in the conduction band,[54] with faster mobilities found for larger crystal sizes. This would imply therefore a shorter charge collection time at the same charge density for photoanodes calcined at higher temperatures, i.e. in larger crystals, consistent with the findings presented in Figure 3. It is important to note that this does not represent an alternative theory for charge transport in mesoporous oxides but is an additional factor to be included when applying the multitrapping model, where $\mu_e$ is usually considered a constant independent of crystal size and morphology.

The multitrapping model limits the parameters that affect charge transport to only the relative occupancy of trapped to free charges. It has been widely debated that other interactions are present, such as band bending at the interface of adjacent nanoparticles, disorder-induced localization of charges, or backscattering of conduction band electrons at the grain boundaries.[24,36,55−57] Although our observed trends are consistent with a pronounced impact of the latter on the long-range mobility of electrons in the conduction band, further work is necessary to develop an extended model that takes these aspects into account.

Whereas the interplay of factors and mechanism governing the charge transport through the film is unclear, it is evident that reducing the number of intergrain boundaries has a positive effect on electron diffusion. This clearly suggests that the manufacture of thick films that can be used in conjunction with panchromatic absorbers requires film morphologies with high enough surface area and a low number of grain boundaries.

In summary, we have examined the factors limiting the diffusion of electrons through mesoporous $TiO_2$ films that were fabricated from block copolymer assembled $TiO_2$. This material route allowed the direct comparison of photoanodes with a nearly constant surface area available for dye anchoring but with a significant range of crystal sizes in the polycrystalline structure. We have found that by increasing the crystal size and reducing the intergrain boundaries, charge transport was accelerated by more than one order of magnitude under constant light intensity and up to three orders of magnitude when compared at the same charge density. In the usual multitrapping model, only systems with significantly different trap density distributions are expected to show differences in charge transport. Here the trap density between samples appears invariant with crystal size, leading us to postulate that the increased crystal sizes lead to higher long-range mobilities of the conduction band electrons. Therefore, previous models describing charge transport in mesoporous $TiO_2$ films require modifications to include not only the population of free charge but also the effects of the intergrain boundaries and other factors influencing the mobility of the electrons in the conduction band. Finally, regardless of the precise charge transport mechanism through the films, our results indicate that maximizing the mesoporous film crystal size while maintaining high enough surface area for dye adsorption should prove to be a viable route for the optimization of charge transport in solid-state DSCs.

## EXPERIMENTAL SECTION

The photoanodes and solid-state DSCs were assembled with the diblock copolymer PI-*b*-PEO, as described in a previous publication.[44] In a typical synthesis, a titania sol is prepared by adding titanium ethoxide to hydrochloric acid. PI-*b*-PEO is then dissolved in tetrahydrofuran (THF) before the titania sol is added. The solution is then cast in a Petri dish, where the solvent is allowed to slowly evaporate at 50 °C. After all of the solvent has evaporated, the mixture is redissolved in an azeotrope solvent mixture of 1-butanol and toluene. This solution is finally spin-coated onto $TiO_2$-coated fluorine-doped tin oxide (FTO) substrates, which are then calcined at a range of temperatures. The photoanodes were then sensitized with the D102 dye[58] and filled with spiro-OMeTAD as the hole transporter and finally silver electrodes were evaporated, as described elsewhere.[11]

Solar-simulated AM 1.5 sunlight was generated with an ABET solar simulator calibrated to give 100 mW $cm^{-2}$ using an NREL-calibrated KG5-filtered silicon reference cell. The $J-V$ curves were recorded with a Keithley 2400. The solar cells were masked with a metal aperture defining the active area of the solar cells. The photovoltage decay measurement was performed by a similar method to O'Regan et al.[59] and as described elsewhere.[48,60,61] Further information can be found in the Supporting Information.

## ASSOCIATED CONTENT

### Supporting Information

Detailed description of the experimental procedure and the photovoltage and photocurrent decay technique is included. This material is available free of charge via the Internet at http://pubs.acs.org.

## AUTHOR INFORMATION

### Corresponding Author

*E-mail: h.snaith1@physics.ox.ac.uk.

## Notes

The authors declare no competing financial interest.

## ■ ACKNOWLEDGMENTS

This project was partially funded by EPSRC and the European Community's Seventh Framework Programme (FP7/2007-2013) under grant agreement no. 246124 of the SANS project.

## ■ REFERENCES

(1) O'Regan, B.; Gratzel, M. A Low Cost, High Efficiency Solar Cell Based On Dye-Sensitised $TiO_2$ Films. *Nature* **1991**, *353*, 737−740.
(2) Hagfeldt, A.; Boschloo, G.; Sun, L. C.; Kloo, L.; Pettersson, H. Dye-Sensitized Solar Cells. *Chem. Rev.* **2010**, *110*, 6595−6663.
(3) Bach, U.; Comte, P.; Moser, J. E.; Weisso, F.; Gratzel, M. Solid-State Dye-Sensitized Mesoporous $TiO_2$ Solar Cells With High Photon-To-Electron Conversion Efficiencies. *Nature* **1998**, *395*, 583−585.
(4) Snaith, H. J. Estimating the Maximum Attainable Efficiency in Dye-Sensitized Solar cells. *Adv. Funct. Mater.* **2010**, *20*, 13−19.
(5) Burschka, J.; Dualeh, A.; Kessler, F.; Baranoff, E.; Cevey-Ha, N.-L.; Yi, C.; Nazeeruddin, M. K.; Gratzel, M. Tris(2-(1H-pyrazol-1-yl)pyridine)cobalt(III) as p-Type Dopant for Organic Semiconductors and Its Application in Highly Efficient Solid-State Dye-Sensitized Solar Cells. *J. Am. Chem. Soc.* **2011**, *133*, 18042−18045.
(6) Snaith, H. J.; Schmidt-Mende, L. Advances In Liquid-Electrolyte And Solid-State Dye-Sensitized Solar Cells. *Adv. Mater.* **2007**, *19*, 3187−3200.
(7) Kruger, J.; Plass, R.; Gratzel, M.; Cameron, P.; Peter, L. Charge Transport and Back Reaction in Solid-State Dye-Sensitized Solar Cells: A Study Using Intensity-Modulated Photovoltage and Photocurrent Spectroscopy. *J. Phys. Chem. B* **2003**, *107*, 7536−7539.
(8) Schmidt-Mende, L.; Grätzel, M. $TiO_2$ Pore-Filling and Its Effect on the Efficiency of Solid-State Dye-Sensitized Solar Cells. *Thin Solid Films* **2006**, *500*, 296−301.
(9) Kroeze, J. E.; Hirata, N.; Schmidt-Mende, L.; Orizu, C.; Ogier, S. D.; Carr, K.; Gratzel, M.; Durrant, J. R. Parameters Influencing Charge Separation in Solid-State Dye-Sensitized Solar Cells Using Novel Hole Conductors. *Adv. Funct. Mater.* **2006**, *16*, 1832−1838.
(10) Ding, I. K.; Tetreault, N.; Brillet, J.; Hardin, B. E.; Smith, E. H.; Rosenthal, S. J.; Sauvage, F.; Gratzel, M.; McGehee, M. D. Pore-Filling of Spiro-OMeTAD in Solid-State Dye Sensitized Solar Cells: Quantification, Mechanism, and Consequences for Device Performance. *Adv. Funct. Mater.* **2009**, *19*, 2431−2436.
(11) Docampo, P.; Hey, A.; Guldin, S.; Gunning, R.; Steiner, U.; Snaith, H. J. Pore Filling of Spiro-OMeTAD in Solid-State Dye-Sensitized Solar Cells Determined Via Optical Reflectometry. *Adv. Funct. Mater.* **2012**, *22*, 5010−5019.
(12) Snaith, H. J.; Gratzel, M. Electron And Hole Transport Through Mesoporous $TiO_2$ Infiltrated With Spiro-OMeTAD. *Adv. Mater.* **2007**, *19*, 3643−3647.
(13) Hauch, A.; Georg, A. Diffusion in the Electrolyte and Charge-Transfer Reaction at the Platinum Electrode in Dye-Sensitized Solar Cells. *Electrochim. Acta* **2001**, *46*, 3457−3466.
(14) Kopidakis, N.; Benkstein, K. D.; van de Lagemaat, J.; Frank, A. J. Transport-Limited Recombination of Photocarriers in Dye-Sensitized Nanocrystalline $TiO_2$ Solar Cells. *J. Phys. Chem. B* **2003**, *107*, 11307−11315.
(15) Abate, A.; Leijtens, T.; Pathak, S.; Teuscher, J.; Avolio, R.; Errico, M. E.; Kirkpatrik, J.; Ball, J. M.; Docampo, P.; McPherson, I.; et al. Lithium Salts As "Redox Active" p-Type Dopants for Organic Semiconductors and Their Impact in Solid-State Dye-Sensitized Solar Cells. *Phys. Chem. Chem. Phys.* **2013**, *15*, 2572−2579.
(16) Bedja, I.; Kamat, P. V.; Hua, X.; Lappin, A. G.; Hotchandani, S. Photosensitization of Nanocrystalline ZnO Films by Bis(2,2′-bipyridine)(2,2;-bipyridine-4,4′-dicarboxylic acid)ruthenium(II). *Langmuir* **1997**, *13*, 2398−2403.
(17) Keis, K.; Magnusson, E.; Lindstrom, H.; Lindquist, S.-E.; Hagfeldt, A. A 5% Efficient Photoelectrochemical Solar Cell Based on Nanostructured ZnO Electrodes. *Sol. Energy Mater. Sol. Cells* **2002**, *73*, 51−58.
(18) Memarian, N.; Concina, I.; Braga, A.; Rozati, S. M.; Vomiero, A.; Sberveglieri, G. Hierarchically Assembled ZnO Nanocrystallites for High-Efficiency Dye-Sensitized Solar Cells. *Angew. Chem., Int. Ed.* **2011**, *50*, 12321−12325.
(19) Kay, A.; Gratzel, M. Dye-Sensitized Core-Shell Nanocrystals: Improved Efficiency of Mesoporous Tin Oxide Electrodes Coated with a Thin Layer of an Insulating Oxide. *Chem. Mater.* **2002**, *14*, 2930−2935.
(20) Tennakone, K.; Bandara, J.; Bandaranayake, P. K. M.; Kumara, G. R. A.; Konno, A. Enhanced Efficiency of a Dye-Sensitized Solar Cell Made from MgO-Coated Nanocrystalline $SnO_2$. *Jpn. J. Appl. Phys., Part 2* **2001**, *40*, L732−L734.
(21) Look, D. C.; Reynolds, D. C.; Sizelove, J. R.; Jones, R. L.; Litton, C. W.; Cantwell, G.; Harsch, W. C. Electrical Properties of Bulk ZnO. *Solid State Commun.* **1998**, *105*, 399−401.
(22) Nagasawa, M.; Shionoya, S.; Makishima, S. Vapor Reaction Growth of $SnO_2$ Single Crystals and Their Properties. *Jpn. J. Appl. Phys.* **1965**, *4*, 195−202.
(23) Forro, L.; Chauvet, O.; Emin, D.; Zuppiroli, L.; Berger, H.; Levy, F. High Mobility n-Type Charge Carriers in Large Single Crystals of Anatase ($TiO_2$). *J. Appl. Phys.* **1994**, *75*, 633−635.
(24) Willis, R. L.; Olson, C.; O'Regan, B.; Lutz, T.; Nelson, J.; Durrant, J. R. Electron Dynamics in Nanocrystalline ZnO and $TiO_2$ Films Probed by Potential Step Chronoamperometry and Transient Absorption Spectroscopy. *J. Phys. Chem. B* **2002**, *106*, 7605−7613.
(25) Fukai, Y.; Kondo, Y.; Mori, S.; Suzuki, E. Highly Efficient Dye-Sensitized $SnO_2$ Solar Cells Having Sufficient Electron Diffusion Length. *Electrochem. Commun.* **2007**, *9*, 1439−1443.
(26) Quintana, M.; Edvinsson, T.; Hagfeldt, A.; Boschloo, G. Comparison of Dye-Sensitized ZnO and $TiO_2$ Solar Cells: Studies of Charge Transport and Carrier Lifetime. *J. Phys. Chem. C* **2006**, *111*, 1035−1041.
(27) Tiwana, P.; Docampo, P.; Johnston, M. B.; Snaith, H. J.; Herz, L. M. Electron Mobility and Injection Dynamics in Mesoporous ZnO, $SnO_2$, and $TiO_2$ Films Used in Dye-Sensitized Solar Cells. *ACS Nano* **2011**, *5*, 5158−5166.
(28) Li, K.-L.; Xie, Z.-B.; Adams, S. Fast Charge Transport of Titania Nanotube Arrays in Dye-Sensitized Solar Cells. *Z. Kristallogr.* **2010**, *225*, 173−179.
(29) Kopidakis, N.; Neale, N. R.; Zhu, K.; van de Lagemaat, J.; Frank, A. J. Spatial Location of Transport-Limiting Traps in $TiO_2$ Nanoparticle Films in Dye-Sensitized Solar Cells. *Appl. Phys. Lett.* **2005**, *87*.
(30) Nakade, S.; Matsuda, M.; Kambe, S.; Saito, Y.; Kitamura, T.; Sakata, T.; Wada, Y.; Mori, H.; Yanagida, S. Dependence of $TiO_2$ Nanoparticle Preparation Methods and Annealing Temperature on the Efficiency of Dye-Sensitized Solar Cells. *J. Phys. Chem. B* **2002**, *106*, 10004−10010.
(31) Nakade, S.; Saito, Y.; Kubo, W.; Kitamura, T.; Wada, Y.; Yanagida, S. Influence of $TiO_2$ Nanoparticle Size on Electron Diffusion and Recombination in Dye-Sensitized $TiO_2$ Solar Cells. *J. Phys. Chem. B* **2003**, *107*, 8607−8611.
(32) Docampo, P.; Guldin, S.; Steiner, U.; Snaith, H. J. Triblock Terpolymer Directed Self-Assembly of Mesoporous $TiO_2$ - High Performance Photoanodes for Solid State Dye-Sensitized Solar Cells. *Adv. Energy Mater.* **2012**, *2*, 676−682.
(33) Zhu, K.; Neale, N. R.; Miedaner, A.; Frank, A. J. Enhanced Charge-Collection Efficiencies and Light Scattering in Dye-Sensitized Solar Cells Using Oriented $TiO_2$ Nanotubes Arrays. *Nano Lett.* **2007**, *7*, 69−74.
(34) Ohsaki, Y.; Masaki, N.; Kitamura, T.; Wada, Y.; Okamoto, T.; Sekino, T.; Niihara, K.; Yanagida, S. Dye-Sensitized $TiO_2$ Nanotube Solar Cells: Fabrication and Electronic Characterization. *Phys. Chem. Chem. Phys.* **2005**, *7*.
(35) van de Lagemaat, J.; Benkstein, K. D.; Frank, A. J. Relation between Particle Coordination Number and Porosity in Nanoparticle

Films: Implications to Dye-Sensitized Solar Cells. *J. Phys. Chem. B* **2001**, *105*, 12433−12436.
(36) Benkstein, K. D.; Kopidakis, N.; van de Lagemaat, J.; Frank, A. J. Influence of the Percolation Network Geometry on Electron Transport in Dye-Sensitized Titanium Dioxide Solar Cells. *J. Phys. Chem. B* **2003**, *107*, 7759−7767.
(37) Orenstein, J.; Kastner, M. Photocurrent Transient Spectroscopy: Measurement of the Density of Localized States in a -$As_2Se_3$. *Phys. Rev. Lett.* **1981**, *46*, 1421−1424.
(38) Tiedje, T.; Rose, A. A Physical Interpretation of Dispersive Transport in Disordered Semiconductors. *Solid State Commun.* **1981**, *37*, 49−52.
(39) Peter, L. M. Dye-Sensitized Nanocrystalline Solar Cells. *Phys. Chem. Chem. Phys.* **2007**, *9*, 2630−2642.
(40) Nelson, J. Continuous-Time Random-Walk Model of Electron Transport in Nanocrystalline $TiO_2$ Electrodes. *Phys. Rev. B* **1999**, *59*, 15374−15380.
(41) Nelson, J.; Chandler, R. E. Random Walk Models of Charge Transfer and Transport in Dye Sensitized Systems. *Coord. Chem. Rev.* **2004**, *248*, 1181−1194.
(42) Bisquert, J.; Vikhrenko, V. S. Interpretation of the Time Constants Measured by Kinetic Techniques in Nanostructured Semiconductor Electrodes and Dye-Sensitized Solar Cells. *J. Phys. Chem. B* **2004**, *108*, 2313−2322.
(43) Guldin, S.; Huttner, S.; Tiwana, P.; Orilall, M. C.; Ulgut, B.; Stefik, M.; Docampo, P.; Kolle, M.; Divitini, G.; Ducati, C.; et al. Improved Conductivity In Dye-Sensitised Solar Cells Through Block-Copolymer Confined $TiO_2$ Crystallisation. *Energy Environ. Sci.* **2011**, *4*, 225−233.
(44) Guldin, S.; Docampo, P.; Stefik, M.; Kamita, G.; Wiesner, U.; Snaith, H. J.; Steiner, U. Layer-by-Layer Formation of Block-Copolymer-Derived $TiO_2$ for Solid-State Dye-Sensitized Solar Cells. *Small* **2011**, *8*, 432−440.
(45) Nedelcu, M.; Lee, J.; Crossland, E. J. W.; Warren, S. C.; Orilall, M. C.; Guldin, S.; Huttner, S.; Ducati, C.; Eder, D.; Wiesner, U.; et al. Block Copolymer Directed Synthesis Of Mesoporous $TiO_2$ For Dye-Sensitized Solar Cells. *Soft Matter* **2009**, *5*, 134.
(46) Guldin, S.; Kolle, M.; Stefik, M.; Langford, R.; Eder, D.; Wiesner, U.; Steiner, U. Tunable Mesoporous Bragg Reflectors Based on Block-Copolymer Self-Assembly. *Adv. Mater.* **2011**, *23*, 3664−3668.
(47) Sanchez, C.; Boissière, C.; Grosso, D.; Laberty, C.; Nicole, L. Design, Synthesis, and Properties of Inorganic and Hybrid Thin Films Having Periodically Organized Nanoporosity. *Chem. Mater.* **2008**, *20*, 682−737.
(48) Docampo, P.; Guldin, S.; Stefik, M.; Tiwana, P.; Orilall, M. C.; Huttner, S.; Sai, H.; Wiesner, U.; Steiner, U.; Snaith, H. J. Control of Solid-State Dye-Sensitized Solar Cell Performance by Block-Copolymer-Directed $TiO_2$ Synthesis. *Adv. Funct. Mater.* **2010**, *20*, 1787−1796.
(49) Miettunen, K.; Barnes, P. R. F.; Li, X.; Law, C.; O'Regan, B. C. The Effect of Electrolyte Filling Method on the Performance of Dye-Sensitized Solar Cells. *J. Electroanal. Chem.* **2012**, *677−680*, 41−49.
(50) O'Regan, B.; Xiaoe, L.; Ghaddar, T. Dye Adsorption, Desorption, And Distribution in Mesoporous $TiO_2$ Films, and Its Effects on Recombination Losses in Dye Sensitized Solar Cells. *Energy Environ. Sci* **2012**, *5*, 7203−7215.
(51) Bisquert, J.; Zaban, A.; Salvador, P. Analysis of the Mechanisms of Electron Recombination in Nanoporous $TiO_2$ Dye-Sensitized Solar Cells. Nonequilibrium Steady-State Statistics and Interfacial Electron Transfer via Surface States. *J. Phys. Chem. B* **2002**, *106*, 8774−8782.
(52) Zhu, K.; Kopidakis, N.; Neale, N. R.; van de Lagemaat, J.; Frank, A. J. Influence of Surface Area on Charge Transport and Recombination in Dye-Sensitized $TiO_2$ Solar Cells. *J. Phys. Chem. B* **2006**, *110*, 25174−25180.
(53) van de Lagemaat, J.; Frank, A. J. Nonthermalized Electron Transport in Dye-Sensitized Nanocrystalline $TiO_2$ Films: Transient Photocurrent and Random-Walk Modeling Studies. *J. Phys. Chem. B* **2001**, *105*, 11194−11205.
(54) Orton, J. W.; Powell, M. J. The Hall Effect in Polycrystalline and Powdered Semiconductors. *Rep. Prog. Phys.* **1980**, *43*, 1263.
(55) Turner, G. M.; Beard, M. C.; Schmuttenmaer, C. A. Carrier Localization and Cooling in Dye-Sensitized Nanocrystalline Titanium Dioxide. *J. Phys. Chem. B* **2002**, *106*, 11716−11719.
(56) Baxter, J. B.; Schmuttenmaer, C. A. Conductivity of ZnO Nanowires, Nanoparticles, and Thin Films Using Time-Resolved Terahertz Spectroscopy. *J. Phys. Chem. B* **2006**, *110*, 25229−25239.
(57) Cai, J.; Han, L. Theoretical Investigation on Interfacial-Potential-Limited Diffusion and Recombination in Dye-Sensitized Solar Cells. *J. Phys. Chem. C* **2011**, *115*, 17154−17162.
(58) Horiuchi, T.; Miura, H.; Sumioka, K.; Uchida, S. High Efficiency of Dye-Sensitized Solar Cells Based on Metal-Free Indoline Dyes. *J. Am. Chem. Soc.* **2004**, *126*, 12218−12219.
(59) O'Regan, B.; Lenzmann, F. Charge Transport and Recombination in a Nanoscale Interpenetrating Network of n-Type and p-Type Semiconductors: Transient Photocurrent and Photovoltage Studies of $TiO_2$/Dye/CuSCN Photovoltaic Cells. *J. Phys. Chem. B* **2004**, *108*, 4342−4350.
(60) Snaith, H. J.; Humphry-Baker, R.; Chen, P.; Cesar, I.; Zakeeruddin, S. M.; Gratzel, M. Charge Collection and Pore Filling in Solid-State Dye-Sensitized Solar Cells. *Nanotechnology* **2008**, *19*, 424003.
(61) Bisquert, J.; Zaban, A.; Greenshtein, M.; Mora-Sero, I. Determination of Rate Constants for Charge Transfer and the Distribution of Semiconductor and Electrolyte Electronic Energy Levels in Dye-Sensitized Solar Cells by Open-Circuit Photovoltage Decay Method. *J. Am. Chem. Soc.* **2004**, *126*, 13550−13559.